Transverse-momentum dependent modification of dynamic texture in central Au+Au collisions at $\sqrt{s_{NN}} = 200$ GeV

J. Adams,[3] M.M. Aggarwal,[29] Z. Ahammed,[43] J. Amonett,[20] B.D. Anderson,[20] D. Arkhipkin,[13] G.S. Averichev,[12] S.K. Badyal,[19] Y. Bai,[27] J. Balewski,[17] O. Barannikova,[32] L.S. Barnby,[3] J. Baudot,[18] S. Bekele,[28] V.V. Belaga,[12] R. Bellwied,[46] J. Berger,[14] B.I. Bezverkhny,[48] S. Bharadwaj,[33] A. Bhasin,[19] A.K. Bhati,[29] V.S. Bhatia,[29] H. Bichsel,[45] A. Billmeier,[46] L.C. Bland,[4] C.O. Blyth,[3] B.E. Bonner,[34] M. Botje,[27] A. Boucham,[38] A.V. Brandin,[25] A. Bravar,[4] M. Bystersky,[11] R.V. Cadman,[1] X.Z. Cai,[37] H. Caines,[48] M. Calderón de la Barca Sánchez,[17] J. Castillo,[21] D. Cebra,[7] Z. Chajecki,[44] P. Chaloupka,[11] S. Chattopdhyay,[43] H.F. Chen,[36] Y. Chen,[8] J. Cheng,[41] M. Cherney,[10] A. Chikanian,[48] W. Christie,[4] J.P. Coffin,[18] T.M. Cormier,[46] J.G. Cramer,[45] H.J. Crawford,[6] D. Das,[43] S. Das,[43] M.M. de Moura,[35] A.A. Derevschikov,[31] L. Didenko,[4] T. Dietel,[14] S.M. Dogra,[19] W.J. Dong,[8] X. Dong,[36] J.E. Draper,[7] F. Du,[48] A.K. Dubey,[15] V.B. Dunin,[12] J.C. Dunlop,[4] M.R. Dutta Mazumdar,[43] V. Eckardt,[23] W.R. Edwards,[21] L.G. Efimov,[12] V. Emelianov,[25] J. Engelage,[6] G. Eppley,[34] B. Erazmus,[38] M. Estienne,[38] P. Fachini,[4] J. Faivre,[18] R. Fatemi,[17] J. Fedorisin,[12] K. Filimonov,[21] P. Filip,[11] E. Finch,[48] V. Fine,[4] Y. Fisyak,[4] K. Fomenko,[12] J. Fu,[41] C.A. Gagliardi,[39] J. Gans,[48] M.S. Ganti,[43] L. Gaudichet,[38] F. Geurts,[34] V. Ghazikhanian,[8] P. Ghosh,[43] J.E. Gonzalez,[8] O. Grachov,[46] O. Grebenyuk,[27] D. Grosnick,[42] S.M. Guertin,[8] Y. Guo,[46] A. Gupta,[19] T.D. Gutierrez,[7] T.J. Hallman,[4] A. Hamed,[46] D. Hardtke,[21] J.W. Harris,[48] M. Heinz,[2] T.W. Henry,[39] S. Hepplemann,[30] B. Hippolyte,[48] A. Hirsch,[32] E. Hjort,[21] G.W. Hoffmann,[40] H.Z. Huang,[8] S.L. Huang,[36] E.W. Hughes,[5] T.J. Humanic,[28] G. Igo,[8] A. Ishihara,[40] P. Jacobs,[21] W.W. Jacobs,[17] M. Janik,[44] H. Jiang,[8] P.G. Jones,[3] E.G. Judd,[6] S. Kabana,[2] K. Kang,[41] M. Kaplan,[9] D. Keane,[20] V.Yu. Khodyrev,[31] J. Kiryluk,[22] A. Kisiel,[44] E.M. Kislov,[12] J. Klay,[21] S.R. Klein,[21] A. Klyachko,[17] D.D. Koetke,[42] T. Kollegger,[14] M. Kopytine,[20] L. Kotchenda,[25] M. Kramer,[26] P. Kravtsov,[25] V.I. Kravtsov,[31] K. Krueger,[1] C. Kuhn,[18] A.I. Kulikov,[12] A. Kumar,[29] R.Kh. Kutuev,[13] A.A. Kuznetsov,[12] M.A.C. Lamont,[48] J.M. Landgraf,[4] S. Lange,[14] F. Laue,[4] J. Lauret,[4] A. Lebedev,[4] R. Lednicky,[12] S. Lehocka,[12] M.J. LeVine,[4] C. Li,[36] Q. Li,[46] Y. Li,[41] G. Lin,[48] S.J. Lindenbaum,[26] M.A. Lisa,[28] F. Liu,[47] L. Liu,[47] Q.J. Liu,[45] Z. Liu,[47] T. Ljubicic,[4] W.J. Llope,[34] H. Long,[8] R.S. Longacre,[4] M. Lopez-Noriega,[28] W.A. Love,[4] Y. Lu,[47] T. Ludlam,[4] D. Lynn,[4] G.L. Ma,[37] J.G. Ma,[8] Y.G. Ma,[37] D. Magestro,[28] S. Mahajan,[19] D.P. Mahapatra,[15] R. Majka,[48] L.K. Mangotra,[19] R. Manweiler,[42] S. Margetis,[20] C. Markert,[48] L. Martin,[38] J.N. Marx,[21] H.S. Matis,[21] Yu.A. Matulenko,[31] C.J. McClain,[1] T.S. McShane,[10] F. Meissner,[21] Yu. Melnick,[31] A. Meschanin,[31] M.L. Miller,[22] N.G. Minaev,[31] C. Mironov,[20] A. Mischke,[27] D.K. Mishra,[15] J. Mitchell,[34] B. Mohanty,[43] L. Molnar,[32] C.F. Moore,[40] D.A. Morozov,[31] M.G. Munhoz,[35] B.K. Nandi,[43] S.K. Nayak,[19] T.K. Nayak,[43] J.M. Nelson,[3] P.K. Netrakanti,[43] V.A. Nikitin,[13] L.V. Nogach,[31] S.B. Nurushev,[31] G. Odyniec,[21] A. Ogawa,[4] V. Okorokov,[25] M. Oldenburg,[21] D. Olson,[21] S.K. Pal,[43] Y. Panebratsev,[12] S.Y. Panitkin,[4] A.I. Pavlinov,[46] T. Pawlak,[44] T. Peitzmann,[27] V. Perevoztchikov,[4] C. Perkins,[6] W. Peryt,[44] V.A. Petrov,[13] S.C. Phatak,[15] R. Picha,[7] M. Planinic,[49] J. Pluta,[44] N. Porile,[32] J. Porter,[45] A.M. Poskanzer,[21] M. Potekhin,[4] E. Potrebenikova,[12] B.V.K.S. Potukuchi,[19] D. Prindle,[45] C. Pruneau,[46] J. Putschke,[23] G. Rakness,[30] R. Raniwala,[33] S. Raniwala,[33] O. Ravel,[38] R.L. Ray,[40] S.V. Razin,[12] D. Reichhold,[32] J.G. Reid,[45] G. Renault,[38] F. Retiere,[21] A. Ridiger,[25] H.G. Ritter,[21] J.B. Roberts,[34] O.V. Rogachevskiy,[12] J.L. Romero,[7] A. Rose,[46] C. Roy,[38] L. Ruan,[36] R. Sahoo,[15] I. Sakrejda,[21] S. Salur,[48] J. Sandweiss,[48] I. Savin,[13] P.S. Sazhin,[12] J. Schambach,[40] R.P. Scharenberg,[32] N. Schmitz,[23] K. Schweda,[21] J. Seger,[10] P. Seyboth,[23] E. Shahaliev,[12] M. Shao,[36] W. Shao,[5] M. Sharma,[29] W.Q. Shen,[37] K.E. Shestermanov,[31] S.S. Shimanskiy,[12] E Sichtermann,[21] F. Simon,[23] R.N. Singaraju,[43] G. Skoro,[12] N. Smirnov,[48] R. Snellings,[27] G. Sood,[42] P. Sorensen,[21] J. Sowinski,[17] J. Speltz,[18] H.M. Spinka,[1] B. Srivastava,[32] A. Stadnik,[12] T.D.S. Stanislaus,[42] R. Stock,[14] A. Stolpovsky,[46] M. Strikhanov,[25] B. Stringfellow,[32] A.A.P. Suaide,[35] E. Sugarbaker,[28] C. Suire,[4] M. Sumbera,[11] B. Surrow,[22] T.J.M. Symons,[21] A. Szanto de Toledo,[35] P. Szarwas,[44] A. Tai,[8] J. Takahashi,[35] A.H. Tang,[27] T. Tarnowsky,[32] D. Thein,[8] J.H. Thomas,[21] S. Timoshenko,[25] M. Tokarev,[12] T.A. Trainor,[45] S. Trentalange,[8] R.E. Tribble,[39] O.D. Tsai,[8] J. Ulery,[32] T. Ullrich,[4] D.G. Underwood,[1] A. Urkinbaev,[12] G. Van Buren,[4] M. van Leeuwen,[21] A.M. Vander Molen,[24] R. Varma,[16] I.M. Vasilevski,[13] A.N. Vasiliev,[31] R. Vernet,[18] S.E. Vigdor,[17] Y.P. Viyogi,[43] S. Vokal,[12] S.A. Voloshin,[46] M. Vznuzdaev,[25] W.T. Waggoner,[10] F. Wang,[32] G. Wang,[20] G. Wang,[5] X.L. Wang,[36] Y. Wang,[40] Y. Wang,[41] Z.M. Wang,[36] H. Ward,[40] J.W. Watson,[20] J.C. Webb,[17] R. Wells,[28] G.D. Westfall,[24] A. Wetzler,[21] C. Whitten Jr.,[8] H. Wieman,[21] S.W. Wissink,[17] R. Witt,[2] J. Wood,[8] J. Wu,[36] N. Xu,[21] Z. Xu,[4] Z.Z. Xu,[36] E. Yamamoto,[21] P. Yepes,[34] V.I. Yurevich,[12] Y.V. Zanevsky,[12] H. Zhang,[4] W.M. Zhang,[20] Z.P. Zhang,[36] P.A Zolnierczuk,[17] R. Zoulkarneev,[13] Y. Zoulkarneeva,[13] and A.N. Zubarev[12]

(STAR Collaboration)

[1]*Argonne National Laboratory, Argonne, Illinois 60439*
[2]*University of Bern, 3012 Bern, Switzerland*
[3]*University of Birmingham, Birmingham, United Kingdom*
[4]*Brookhaven National Laboratory, Upton, New York 11973*
[5]*California Institute of Technology, Pasadena, California 91125*
[6]*University of California, Berkeley, California 94720*
[7]*University of California, Davis, California 95616*
[8]*University of California, Los Angeles, California 90095*
[9]*Carnegie Mellon University, Pittsburgh, Pennsylvania 15213*
[10]*Creighton University, Omaha, Nebraska 68178*
[11]*Nuclear Physics Institute AS CR, 250 68 Řež/Prague, Czech Republic*
[12]*Laboratory for High Energy (JINR), Dubna, Russia*
[13]*Particle Physics Laboratory (JINR), Dubna, Russia*
[14]*University of Frankfurt, Frankfurt, Germany*
[15]*Institute of Physics, Bhubaneswar 751005, India*
[16]*Indian Institute of Technology, Mumbai, India*
[17]*Indiana University, Bloomington, Indiana 47408*
[18]*Institut de Recherches Subatomiques, Strasbourg, France*
[19]*University of Jammu, Jammu 180001, India*
[20]*Kent State University, Kent, Ohio 44242*
[21]*Lawrence Berkeley National Laboratory, Berkeley, California 94720*
[22]*Massachusetts Institute of Technology, Cambridge, MA 02139-4307*
[23]*Max-Planck-Institut für Physik, Munich, Germany*
[24]*Michigan State University, East Lansing, Michigan 48824*
[25]*Moscow Engineering Physics Institute, Moscow Russia*
[26]*City College of New York, New York City, New York 10031*
[27]*NIKHEF, Amsterdam, The Netherlands*
[28]*Ohio State University, Columbus, Ohio 43210*
[29]*Panjab University, Chandigarh 160014, India*
[30]*Pennsylvania State University, University Park, Pennsylvania 16802*
[31]*Institute of High Energy Physics, Protvino, Russia*
[32]*Purdue University, West Lafayette, Indiana 47907*
[33]*University of Rajasthan, Jaipur 302004, India*
[34]*Rice University, Houston, Texas 77251*
[35]*Universidade de Sao Paulo, Sao Paulo, Brazil*
[36]*University of Science & Technology of China, Anhui 230027, China*
[37]*Shanghai Institute of Applied Physics, Shanghai 201800, China*
[38]*SUBATECH, Nantes, France*
[39]*Texas A&M University, College Station, Texas 77843*
[40]*University of Texas, Austin, Texas 78712*
[41]*Tsinghua University, Beijing 100084, China*
[42]*Valparaiso University, Valparaiso, Indiana 46383*
[43]*Variable Energy Cyclotron Centre, Kolkata 700064, India*
[44]*Warsaw University of Technology, Warsaw, Poland*
[45]*University of Washington, Seattle, Washington 98195*
[46]*Wayne State University, Detroit, Michigan 48201*
[47]*Institute of Particle Physics, CCNU (HZNU), Wuhan 430079, China*
[48]*Yale University, New Haven, Connecticut 06520*
[49]*University of Zagreb, Zagreb, HR-10002, Croatia*

(Dated: January 10, 2005)

Correlations in the hadron distributions produced in relativistic Au+Au collisions are studied in the discrete wavelet expansion method. The analysis is performed in the space of pseudorapidity ($|\eta| \leq 1$) and azimuth (full 2π) in bins of transverse momentum (p_t) from $0.14 \leq p_t \leq 2.1$ GeV/c. In peripheral Au+Au collisions a correlation structure ascribed to minijet fragmentation is observed. It evolves with collision centrality and p_t in a way not seen before which suggests strong dissipation of minijet fragmentation in the longitudinally-expanding medium.

PACS numbers: 24.60.Ky, 25.75.Gz, 25.75.-q

The study of the bulk properties of strongly interacting matter under extreme conditions at the Relativistic Heavy Ion Collider (RHIC) is producing a number of tantalizing results [1]. The physics of central Au+Au collisions at RHIC is clearly much more complex than a mere independent superposition of nucleon-nucleon collisions,

while the issues of possible collectivity and of the degree of "thermalization" of the bulk hadronic medium remain open. Substantial equilibration, especially in a short-lived finite system, may imply that during the evolution, there was a large number of degrees of freedom involved, such as would occur in a partonic medium [2] or quark-gluon plasma [3]. Equilibration in heavy ion collisions has been studied *via* its effects on single particle spectra and identified particle ratios. It progressively erases correlations, starting with the smallest features [4, 5]. Surviving correlations produced by hard scatterings early in the collision provide a sensitive monitor of the degree of equilibration of the medium. In contrast, traversal of the QCD phase boundary may *create* specific dynamical correlations [6]. Therefore correlations observed in the final state are potentially affected by competing mechanisms. This makes the question of equilibration a quantitative one and warrants a study of correlations among the majority of hadrons over a range of momentum scales. This Letter reports such a study.

In high energy elementary collisions, hadrons originate from the fragmentation of a color-neutral system of partons. In these systems correlations are produced by local conservation of charge, flavor, energy and momentum in the strong interaction, and by quantum statistics. In high energy heavy ion collisions aspects of these elemental correlations might persist, especially at high transverse momentum (p_t) since the "memory" of the early hard partonic scattering is not easily erased there. In contrast, minijets [7] at lower p_t are expected to have shorter mean free paths in the medium and thus are more likely to dissipate, erasing correlations. The collision overlap density and size of the interaction volume are changed by varying the centrality, which might also control the degree of equilibration in these systems. We study the correlation structure in peripheral collisions, caused by minijets, which evolves with centrality and p_t in a manner suggesting strong dissipation of minijet fragmentation by the longitudinally expanding medium.

The data presented here were obtained with the STAR Time Projection Chamber (TPC) [8], mounted inside a solenoidal magnet. Charged-particle tracking with the TPC covers large acceptance well suited for precision studies of correlation structures over a wide range of scales. The minimum-bias event trigger discriminates on a neutral-spectator signal in the Zero Degree Calorimeters [9]. Central events were selected by additionally requiring a high charged particle multiplicity within $|\eta| < 1$ in the Central Trigger Barrel scintillators [8]. Accepted charged-particle tracks had > 15 TPC space points and $>52\%$ of the estimated maximum possible number of space points (to eliminate split tracks), passed within 3 cm of the event vertex and were within the kinematic acceptance: $|\eta| \leq 1$, full 2π in azimuth, and $0.14 \leq p_t \leq 2.1$ GeV/c. Accepted events had their primary vertex within 25 cm of the geometric center of the TPC longitudinally and had $\geq$15 accepted TPC tracks. About 0.6 M central and 0.3 M peripheral events, recorded in the $\sqrt{s_{NN}} = 200$ GeV run, were analyzed.

Two-point correlations and power spectra of point-to-point fluctuations are complementary measures used to study the correlation structure of random fields (such as TPC events). The former has computational complexity $O(N^2)$ (N is event multiplicity). The latter, implemented via the discrete wavelet transform (DWT) method, is $O(N)$. The DWT-based dynamic texture measure, defined below, is used in this work and was originally applied to relativistic Pb+Pb collisions by NA44 [10].

In this approach, the measured particle distribution $\rho(\phi, \eta)$ *in a single event* is expanded in the complete orthonormal wavelet basis of Haar [11]. The scale of this basis is defined by the *scaling function* $g(x) = 1$ for $0 \leq x < 1$ and 0 otherwise. The function $f(x) = \{1 \text{ for } 0 \leq x < 0.5; -1 \text{ for } 0.5 \leq x < 1; \text{ else } 0\}$ is the wavelet function. The experimental acceptance in η, ϕ, and p_t is split into equal bins in η,ϕ and p_t bins exponentially growing to equalize bin statistics. To keep notation simple but explicit, we introduce $\eta' \equiv (\eta + 1)/2$ and $\phi' \equiv \phi/2\pi$ so that $\eta', \phi' \in [0, 1]$. The scaling function of the Haar basis in two dimensions $G(\phi, \eta) = g(\phi')g(\eta')$ is just the bin acceptance (modulo units). The wavelet functions F^λ (the directional sensitivity mode λ is either along azimuth ϕ, pseudo-rapidity η, or diagonal $\phi\eta$ directions) are $F^{\phi\eta} = f(\phi')f(\eta')$, $F^\phi = f(\phi')g(\eta')$, $F^\eta = g(\phi')f(\eta')$. We define a two dimensional wavelet basis:

$$F^\lambda_{m,i,j}(\phi, \eta) = 2^m F^\lambda(2^m\phi' - i, 2^m\eta' - j), \qquad (1)$$

where $m \geq 0$ is the integer scale fineness index [12], integers i and j index the positions of bin centers in ϕ' and η', and $0 \leq i, j < 2^m$. Scaling functions $G_{m,i,j}(\phi, \eta)$ are constructed analogous to Eq.1. Arbitrary density $\rho(\phi, \eta)$ is expanded as

$$\rho(\phi, \eta) = \langle \rho, G_{0,0,0}\rangle G_{0,0,0} + \sum_{m,i,j,\lambda} \langle \rho, F^\lambda_{m,i,j}\rangle F^\lambda_{m,i,j}, \quad (2)$$

where $\langle \rho, G\rangle$ and $\langle \rho, F^\lambda\rangle$ are expansion coefficients obtained by projecting density $\rho(\phi, \eta)$ onto the basis functions.

In practice $m \leq m_{\max}$, where $m_{\max}$ is the finest scale limited by track resolution and, due to the needs of event mixing, by the number of available events. The coarser scales correspond to successively re-binning the track distribution. The analysis is best visualized by considering the scaling function $G_{m,i,j}(\phi, \eta)$ as binning the track distribution $\rho(\phi, \eta)$ in bins i,j of given fineness m, while the wavelet expansion coefficients $\langle \rho, F^\lambda_{m,i,j}\rangle$ give the difference distribution for data with binning one step finer. The wavelet expansion coefficients were calculated using the code WAILI [13].

The *power spectrum* is defined as

$$P^\lambda(m) = 2^{-2m}\overline{\sum_{i,j} \langle \rho, F^\lambda_{m,i,j}\rangle^2}, \qquad (3)$$

where the overline denotes an average over events. $P^\lambda(m)$ is independent of m for an uncorrelated ρ. However, for physical events P^λ depends on m due to the presence of *static texture* features such as acceptance asymmetries and imperfections (albeit minor in STAR), and non-uniformity of $dN/\,d\eta$. To remove these known features from the analysis a reference is constructed from mixed events starting with individual (ϕ, η) pixels of true events at the finest scale used in the analysis (16×16). A "mixed event" consists of 16×16 (ϕ, η) pixels from true events, where each pixel is taken from different, but similar, real events. The power spectrum $P^\lambda_{\rm mix}$ is obtained from Eq. 3 using the expansion coefficients in Eq. 2. $P^\lambda_{\rm mix}$ contains static, experimental track density artifacts plus statistical noise. The quantity of interest is the difference, $P^\lambda_{\rm dyn} \equiv P^\lambda_{\rm true} - P^\lambda_{\rm mix}$, called *dynamic texture* [10].

In studying the dynamic texture data as a function of p_t, the desirable normalization is such that the results are independent of p_t bin size under the assumption of large-scale correlations in p_t (*i.e.* larger than the p_t acceptance). In this case for increasing number of particles N in an increasing p_t bin, $P^\lambda_{\rm dyn} \propto N^2$ while $P^\lambda_{\rm mix} \propto N$, being a Poissonian variance. Therefore we present the data as the combined quantity $P^\lambda_{\rm dyn}/P^\lambda_{\rm mix}/N$.

Systematic error can be introduced in $P^\lambda_{\rm dyn}$ by the process of event mixing. For example, events with different vertex positions along the beam axis are reconstructed with slightly different efficiencies and acceptances with respect to η. This variable efficiency may fake a dynamic texture effect in η. In order to minimize such errors, events were grouped into event classes with similar multiplicity (within 50) and vertex position (within 10 cm). $P^\lambda_{\rm dyn}$ was constructed using only events within each of these two classes. Results showed no vertex dependence. The upper limit on the systematic error due to z-vertex position variation is set by the statistical error of the data, shown in the figures.

Event centrality in this analysis is characterized by the accepted number of quality tracks in the TPC and expressed as a percentage of the total inelastic cross-section, as before[14]. Event classes in multiplicity are grouped to form two centrality classes: *central*, with 4% of the most central events, and *peripheral*, with event centrality varying between 60% and 84%. The HIJING [15] generator events for the Monte Carlo comparison are selected to match these centrality ranges.

Track splitting (one particle reconstructed as > 1 track) contributions were eliminated by track quality requirements. Track merging (> 1 particles reconstructed as one track) mocks up anticorrelations and can induce systematic error. To estimate this effect, central HIJING events were filtered with an algorithm emulating track recognition properties of the TPC [16]. The simulation results can be expressed as a set of coefficients relating $P_{\rm true}$, $P_{\rm mix}$ and $dN/\,dp_t$ in the original and filtered HIJING data. An estimate of track merging effects in the data was obtained from the inverse of these coefficients. The resulting systematic error was estimated

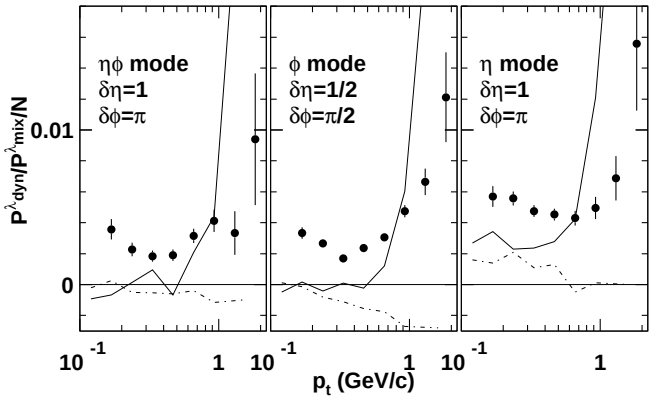

FIG. 1: Peripheral events: normalized dynamic texture for fineness scales $m = 0, 1, 0$ from left to right panels, respectively, as a function of p_t. • – STAR data; solid line – HIJING without jet quenching; dash-dotted line – HIJING without jets.

to be 0.5×10^{-4}. Systematic error due to non-primary background was estimated assuming that the correlations between true primary and non-primary particles could be anything from zero to that of primary particles themselves. The systematic error estimate was taken to be half the difference between these two limits which is 10% of the signal at $p_t = 0.2$ GeV/c, falling to 3.5% at $p_t = 1$ GeV/c. This estimate applies to both centrality classes.

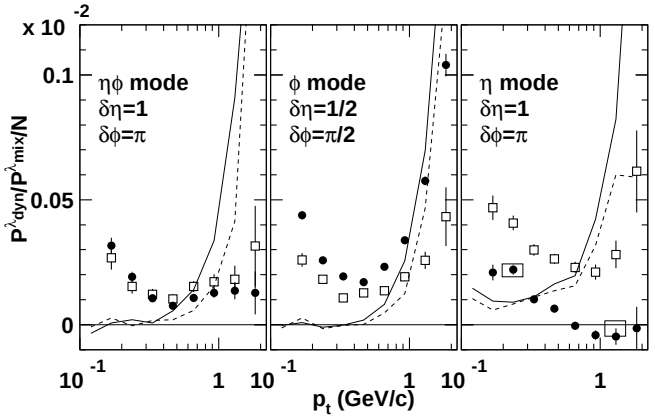

FIG. 2: Central events: normalized dynamic texture for fineness scales $m = 0, 1, 0$ from left to right panels, respectively, as a function of p_t. • – STAR data; solid line – HIJING without jet quenching; dashed line – HIJING with quenching; □ – peripheral STAR data from Fig. 1 renormalized as described in the text. The rectangles around two chosen points show the estimated systematic errors.

Fig. 1 presents measured large-scale dynamic texture in peripheral collisions compared with HIJING predictions where fineness scale $m = 0$ is used for the $\eta\phi$ and η modes and fineness $m = 1$ is used for the ϕ mode. The finer scale for $\delta\phi$ is used so that the angular coverages subtended by $\delta\phi$ for $m = 1$ and $\delta\eta$ for $m = 0$ are comparable. This scale, with ϕ-bin size $\delta\phi = \pi/2$ [12], is

dominated by elliptic flow [17]. The HIJING calculations without jet quenching show a region of approximately constant signal near $p_t \sim 0.5$ GeV/c followed by an increase for $p_t > 0.8$ GeV/c, obtained by "turning on" jets in the model. In that p_t range the STAR data also increase with p_t. Momentum conservation suppresses the difference in the numbers of tracks emitted in the opposite directions. This effect is absent in the mixed events, resulting in negative $P^{\lambda}_{\rm dyn}$, seen in ϕ when jets in HIJING are "off". Comparing the two simulations in Fig. 1 we conclude that fluctuations in local hadron density due to jets are observable in peripheral RHIC collisions at $0.8 < p_t < 2$ GeV/c. This supports but does not prove the identification of similar signals in the data at these p_t with minijets. Without ruling out other sources of angular correlations at such p_t, we use Occam's razor to adopt the well established effect – fragmentation of semi-hard scattering products (jets or minijets) – as the explanation.

Central event data and HIJING predictions with and without jet quenching are shown in Fig. 2. The most striking difference here compared to the peripheral data in Fig. 1 is the reduction in the magnitude of the $P^{\eta}_{\rm dyn}$ at larger $p_t > 0.6$ GeV/c, the data becoming slightly negative near 1 GeV/c in sharp contrast to the jet-like behavior predicted by HIJING. The perturbative partonic energy loss model of jet quenching in HIJING seems to miss the correlation aspect of the picture, at least at these p_t. In the absence of a successful theory to describe the effect, we formulate and test a "null hypothesis": the correlation structure $P^{\lambda}_{\rm dyn}/P^{\lambda}_{\rm mix}$ in Au+Au collisions is independent of centrality. Then, the difference in $P^{\lambda}_{\rm dyn}/P^{\lambda}_{\rm mix}/N$ in central and peripheral events (including the p_t trends) is due to the difference in $1/N$ (*i.e.* in $dN/\,dp_t$, for $N \equiv N(p_t) = \int_{p_t\,\rm bin} dN(p_t)$) [18]. Shown in Fig. 2 as symbol $\Box$ are the peripheral data from Fig. 1, rescaled under an assumption of the "null hypothesis" by $\times N(p_t)|_{\rm periph}/N(p_t)|_{\rm centr}$. The left panel shows that the $\eta\phi$-mode is less affected by centrality, reflecting a superposition of the opposite centrality trends in η and ϕ. We hypothesize that the deviation of the STAR data from the "null hypothesis" in η in the otherwise correlated system points to a *randomization* (dissipation) of minijet structure in the longitudinal direction. Longitudinal expansion of the hot, dense medium formed early in the collision singles out the η direction and is likely to be part of the dissipation mechanism. If so, at $p_t > 0.6$ GeV/c we may be observing an effect of the longitudinally expanding medium on parton fragmentation or hadronization.

In each panel of Figs. 1 and 2 the dynamic texture data increase with decreasing p_t for $p_t < 0.4$ GeV/c. Data stay non-zero at low p_t for all three modes in the experiment and for the η-mode in HIJING. In this p_t range, the correlations are likely dominated by centrality-dependent effects such as the final state quantum statistical intensity interference, Coulomb effect and longitudinal string fragmentation physics, simulated in HIJING. Modification of the latter effect with centrality is the subject of a separate publication[19].

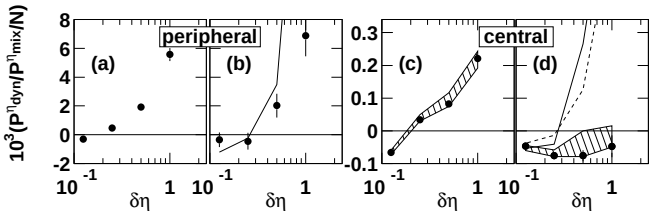

FIG. 3: Scale dependence of the dynamic texture in peripheral and central events.(a,c): $0.2 < p_t < 0.28$, (b,d): $1.1 < p_t < 1.5$ GeV/c. • – STAR data; solid line – HIJING without jet quenching; dashed line – HIJING with quenching. A systematic error estimate is shown as a hatched area. Errors on different scales are estimated independently.

Fig. 3 shows a scale dependence of the η-mode in the low and higher p_t intervals. At low p_t, the peripheral and central trends qualitatively agree, whereas at higher p_t, a modification with centrality is seen, which testifies to the presence of new physics at higher p_t. The reduction of the dynamic texture in central events with respect to both HIJING and the peripheral STAR data is most dramatic at the coarser scales. The longitudinal expansion correlates η with the longitudinal coordinate z, and z – with time. Final state particles with large $\delta\eta$ are more likely to be separated by a space-like interval. Thus, the larger $\delta\eta$ correlations are more likely to have their cause in the particles' common past, reflecting the early stage of the system, whereas the fine scale features are formed later under conditions little different from peripheral collisions or conventional hadronic models. The negative $P^{\eta}_{\rm dyn}$ in Fig. 3(d) points to the presence of an anticorrelation mechanism, which could include existence of a characteristic scale in the longitudinal separation of hadrons in the course of hadronization. Lack of scale dependence in Fig. 3(d), relative to Fig. 3(b), may be contrasted with progressive reduction of small-scale Fourier harmonics from hadronic diffusion discussed in [5]. Alternatively, pre-hadronic transport on η involving partonic diffusion could provide a more efficient equilibration mechanism. Other mechanisms such as convective turbulent transport [20] might also play a role. The reduction of dynamic texture reported in this Letter provides a new quantitative argument in favor of equilibration or dissipation effects. However, we observe that the hadronic final state is not correlation free, even for central events.

In summary, a non-trivial picture emerges when the DWT power spectrum technique is applied for the first time to Au+Au collision data from RHIC. Large-scale ($\delta\eta = 1$) angular correlations for $p_t < 2.1$ GeV/c are observed in peripheral events and identified with minijets. In central events, those correlations are suppressed with increasing p_t and $\delta\eta$. This indicates a major change in the properties of the medium with increasing collision centrality, implying the development of a dissipative medium. In the course of its longitudinal expansion, this

hypothetic medium influences via interactions the structure of correlations, inherited from the kinematics of the initial-state semi-hard scattering, causing their dissipation and partial equilibration.

We thank the RHIC Operations Group and RCF at BNL, and the NERSC Center at LBNL for their support. This work was supported in part by the HENP Divisions of the Office of Science of the U.S. DOE; the U.S. NSF; the BMBF of Germany; IN2P3, RA, RPL, and EMN of France; EPSRC of the United Kingdom; FAPESP of Brazil; the Russian Ministry of Science and Technology; the Ministry of Education and the NNSFC of China; Grant Agency of the Czech Republic, FOM and UU of the Netherlands, DAE, DST, and CSIR of the Government of India; Swiss NSF; and the Polish State Committee for Scientific Research.

[1] T. Ludlam and L. McLerran, Physics Today, October 2003, pg. 48, and references therein.
[2] E. L. Feinberg, Sov. Phys. Usp. **26**, 1 (1983) [Usp. Fiz. Nauk **139**, 3 (1983)].
[3] J. C. Collins and M. J. Perry, Phys. Rev. Lett. **34**, 1353 (1975).
[4] T. A. Trainor, arXiv:hep-ph/0001148
[5] E. V. Shuryak and M. A. Stephanov, Phys. Rev. C **63**, 064903 (2001)
[6] L. Van Hove, Z. Phys. C **27**, 135 (1985); M. A. Stephanov, K. Rajagopal and E. V. Shuryak, Phys. Rev. Lett. **81**, 4816 (1998); K. Rajagopal and F. Wilczek, Nucl. Phys. B **399**, 395 (1993).
[7] K. Kajantie, P. V. Landshoff and J. Lindfors, Phys. Rev. Lett. **59**, 2527 (1987), and references therein.
[8] M. Anderson *et al.*, Nucl. Instrum. Meth. A **499**, 659 (2003).
[9] C. Adler, A. Denisov, E. Garcia, M. Murray, H. Strobele and S. White, Nucl. Instrum. Meth. A **499**, 433 (2003).
[10] I. Bearden *et al.*, Phys. Rev. C. **65**, 044903 (2002).
[11] I. Daubechies, *Ten Lectures on Wavelets* (SIAM, Philadelphia, 1992) and references therein.
[12] We specify scale by the m index or by the bin size δx in the space of kinematic variable x. For acceptance Δx, scale (bin size) $\delta x = \Delta x/2^{m+1}$, $m \geq 0$.
[13] G. Uytterhoeven *et al.*, WAILI: Wavelets with Integer Lifting. TW Report 262, Department of Computer Science, Katholieke Universiteit Leuven, Belgium, July 1997.
[14] C. Adler *et al.*, Phys. Rev. Lett. **89**, 202301 (2002)
[15] X. N. Wang and M. Gyulassy, Phys. Rev. D **44**, 3501 (1991); M. Gyulassy and X. N. Wang, Comput. Phys. Commun. **83**, 307 (1994). We use version 3.82 of the model.
[16] The algorithm merges close tracks, based on known close track recognition efficiencies in STAR, where all two-track separation distances are evaluated at three radii in the TPC; close pairs are merged.
[17] K. H. Ackermann *et al.*, Phys. Rev. Lett. **86**, 402 (2001).
[18] This hypothesis is not identical with assuming that A+A collisions are a superposition of independent NN collisions – the latter assumption excludes modifications of p_t spectra with centrality, which we allow.
[19] J. Adams *et al.*, arXiv:nucl-ex/0406035.
[20] P. Carruthers, in: *First International Workshop on Local Equilibrium in Strong Interaction Physics*, edited by D.K. Scott, and R.M. Weiner (World Scientific, Singapore, 1985).